

Planar buckling controlled optical conductivity of SiC monolayer from Deep-UV to visible light region: A first-principles study

Nzar Rauf Abdullah^{a,b}, Hunar Omar Rashid^a, Botan Jawdat Abdullah^c, Chi-Shung Tang^d, Vidar Gudmundsson^e

^a*Division of Computational Nanoscience, Physics Department, College of Science, University of Sulaimani, Sulaimani 46001, Kurdistan Region, Iraq*

^b*Computer Engineering Department, College of Engineering,*

Komar University of Science and Technology, Sulaimani 46001, Kurdistan Region, Iraq

^c*Physics Department, College of Science- Salahaddin University-Erbil, Erbil 44001, Kurdistan Region, Iraq*

^d*Department of Mechanical Engineering, National United University, 1, Lienda, Miaoli 36003, Taiwan*

^e*Science Institute, University of Iceland, Dunhaga 3, IS-107 Reykjavik, Iceland*

Abstract

The electrical and optical properties of flat and planar buckled siligraphene (SiC) monolayer are examined using a first principles approach. Buckling between the Si and the C atoms in SiC structures influences and impacts the properties of the 2D nanomaterial, according to our results. The electron density of a planar SiC monolayer is calculated, as well as the effects of buckling on it. According to our findings, a siligraphene monolayer is a semiconductor nanomaterial with a direct electronic band gap that decreases as the planar buckling rises. The contributions to the density of states differ owing to changes in the system's structure. Another explanation is that planar buckling reduces the sp^2 overlapping, breaking the bond symmetry causing it to become a sp^3 bond. We show that increased planar buckling between the Si and the C atoms alters the monolayer's optical, mechanical, and thermal properties. A managed planar buckling increases the optical conductivity with a significant shift in the far visible range, as all optical spectra features are red shifted, still remaining visible. Instead of a σ - σ covalent bond, the sp^3 hybridization produces a stronger σ - π bond. Optical characteristics such as the dielectric function, the absorbance, and the optical conductivity of a SiC monolayer are investigated for both parallel and perpendicular polarization of the incoming electric field for both flat and planar buckled systems. The findings show that the optical properties are influenced for both of these two polarizations, with a significant change in the optical spectrum from the near visible to the far visible. The ability to manipulate the optical and electrical characteristics of this critical 2D material through planar buckling opens up new technological possibilities, especially for optoelectronic devices.

Keywords: SiC (Siligraphene) monolayers, DFT, Electronic structure, Optical properties

1. Introduction

Nanomaterials are important in the development of a wide range of modified-material devices, and their high specific surface areas and unique physical properties will make them useful in application. Two-dimensional (2D) monolayers are important in today's research due to their improved magnetic, electrical, optical, mechanical, and catalytic properties compared to their bulk form [1–3]. One of the most essential characteristics that distinguishes nanomaterials from other materials is their dimensionality. Graphene [4], the first 2D monolayer, was discovered in 2004, but other materials have also been synthesized experimentally [5–8].

Novel 2D materials with modest band gaps, high carrier mobilities, and great stability are highly wanted for applications. Among them, the siligraphene monolayer, a

2D form of silicon carbide, is one of the most fascinating SiC, that can be used in a range of applications. Carbon, the main component of graphene, tends to form sp^2 hybridization in 2D structures, which are plentiful and safe on Earth. Silicon, on the other hand, is the semiconductor industry's present basis. Both components are low-cost resources, that are an ideal options for building optical applications. Siligraphene monolayers with varying Si/C concentrations have surpassed pure graphene and silicene with improved mechanical, electrical, optical, and thermodynamic properties [9–14].

Many attempts have been made to experimentally synthesize siligraphene monolayers, including nanocleavage exfoliation in polar solutions like N-methylpyrrolidone and isopropyl alcohol to reduce SiC to a single layer or few layers with thicknesses as low as 0.5–1.5 nm, according to findings reported in the literature. These ultrathin free-standing SiC sheets, which are made composed of graphitic SiC, graphene, and embedded ultrathin wurtzite SiC, have excellent photoluminescence properties [15]. In another

Email address: nzar.r.abdullah@gmail.com (Nzar Rauf Abdullah)

study, distinct 2D SiC nanosheets with an average inter-layer distance of 0.255 nm were created by combining a carbothermal reaction with a post-sonication phase. The average thickness of the free-standing nanosheets was found to be 2-3 nm [16]. A reactive sintering technology based on a two-step sintering procedure in the [111] direction was successfully used to generate SiC nanosheets with an average thickness of 33.7 nm on original graphite surfaces [17], and a wet exfoliation process was applied for the first time in 2021 to successfully separate 2D SiC from hexagonal SiC. Unlike many other 2D materials, such as silicene, which tends to deteriorate, the 2D SiC nanosheets developed are stable and exhibit no signs of degradation. According to a study, the fabricated 2D SiC also generates visible light [18].

The ability to fine-tune the material properties of a monolayer opens the door to a wide range of applications. Many approaches, including the use of doping, strain, electric field, and the tuning of planar buckling, have been proposed theoretically to effectively control their essential properties. Doping is a way for fine-tuning a material's electronic structure and other characteristics. The dopants are transition metals (Ti, V, Cr, Mn, and Fe) in the SiC monolayers that have been studied using density functional theory to investigate their structural, electrical, and magnetic properties. These dopants changed the host's electrical and magnetic properties by generating gap states inside the SiC's band structure [19]. The electrical structure and the optical properties of rare earth atoms doped in SiC monolayers, such as La, Ce, and Th, are investigated using the first-principle approach. Pure 2D SiC is a direct-gap semiconductor with a gap of 2.60 eV. The La-doping of a 2D SiC introduces an impurity states at the Fermi energy, and the band gap is 1.93 eV, after a doping where Si atoms are replaced with rare earth atoms. They become quasi-direct band-gap semiconductors when Ce or Th is added to them. Doping with La increases the static dielectric constant of 2D SiC, whereas Th has minimal effects [20].

The characteristics of a 2D monolayer can be influenced by both strain and electric fields. Density functional theory calculations have been employed to investigate the structural, the electrical, and the optical characteristics of a layered SiC monolayer, that has been modified for in-plane or out-of-plane strain effects. Strain may be used to generate a tunable band structure and optical properties, such as indirect-direct band gap transitions, band gap shrinking and enlargement, and red or blue shifts of absorption peaks [21, 22]. The structure of SiC monolayers under unidirectional strain regimes has been explored using density functional calculations. The material deforms anisotropically in the stress domain, exhibiting non-linear elastic deformation. Under compressive 10.35 percent strain, the indirect band gap of a 2D SiC monolayer turns to a direct band gap, and at 16.87 percent, it becomes a metal. In addition, structural-electronic-bonding findings show that the design of a band gap may be con-

trolled by using a unidirectional strain regime to reduce the band gap [23].

On the other hand, the gas-sensing capabilities of SiC monolayer can be improved by functionalizing the materials, such as by adding an external electric field. According to first-principles considerations, the SiC₇ monolayer is optimal for use as a gas sensing material for detecting NO, NO₂, and NH₃. Furthermore, the applied electric field can change the electrical and optical characteristics of molecules adsorbed on the SiC₇ monolayer [24], and The effect of hydrogen adsorption on the SiC monolayer was studied using density-functional theory approach, which took into account several adsorption process configurations. Despite having almost comparable electrical characteristics, the chair-like shape is found to be more stable, with a binding energy of roughly -3.845 eV for hydrogen atoms. Owing to hydrogen adsorption the plasmon frequency of the chair-like, hydrogenated monolayer is shifted and the optical characteristics changed producing a drop in the dielectric constant and the static refractive index [25].

Another fascinating way of modifying physical features is a planar buckling modification. Buckling effects on the electrical and optical characteristics of beryllium oxide monolayers were previously investigated using a first-principles approach with moderate planar buckling. Planar buckling can lead to a variation of the band gap, according to electrical investigations, since the energy band gap reduces when the planar buckling parameter is increased. Furthermore, increasing the planar buckling factor leads to red-shift of all optical spectra features to lower energy [26]. The electrical and optical properties of a hexagonal boron nitride monolayer have been investigated using a density functional analysis to modify the planar buckling. As a result, the wide band gap of a flat BN monolayer is reduced to a narrower band gap in a buckled BN monolayer, improving optical activity in the Deep-UV region. Additionally, increased planar buckling enhances the optical conductivity in both the visible and the deep-UV domains, depending on the polarization orientation of the incoming light [27].

In this work, the electrical and optical characteristics of SiC monolayers are investigated using first-principles calculations for flat and buckled structures with a range of planar buckling values. We find that planar buckling of SiC monolayers can generate a variable band gap, which decreases as the planar buckling increases. All related impact factors, such as the tuning of the density of state, the elongation of the bond length between the Si and C, and the change in the charge density distribution, are analyzed for structural modification. All key parameters such as the dielectric function, the absorption coefficient, and the optical conductivity change and are examined when the planar buckling factor is enhanced. Our findings give rise to new information about optoelectronic functionality in nanotechnology.

The computational methodologies and model structure

are briefly discussed in Sec. 2. The major achieved outcomes are examined in Sec. 3. The conclusion of the results is reported in Sec. 4

2. Methodology

We consider a 2D SiC monolayer structure consisting of a 2×2 supercell with equal number of Si and C atoms. The SiC monolayer is fully relaxed with the plane-waves kinetic energy and charge densities cutoff assumed to be 1088.5 eV, and 1.088×10^4 eV, respectively. The SiC monolayer is relaxed until all the forces on the atoms are less than 10^{-5} eV/Å with a $18 \times 18 \times 1$ Monkhorst-Pack grid. The interaction of individual SiC monolayers is canceled out by assuming a large wide vacuum layer of 20 Å in the z -direction. The generalized gradient approximation (GGA) with the Perdew-Burke-Ernzerhof (PBE) functionals is used to approximate the exchange and the correlation term [28]. The GGA-PBE is implemented in the Quantum espresso (QE) software [29, 30]. The DFT approach in the QE software is implemented based on the Kohn-Sham density functional theory (KS-DFT). The band structure and the density of states (DOS) are obtained by utilizing the Self-Consistent Field (SCF) and non-self-consistent field (NSCF) calculations, respectively. In these calculations, we have used a Monkhorst-Pack grid of $18 \times 18 \times 1$ for the SCF and $100 \times 100 \times 1$ for the NSCF. The optical properties of the SiC monolayers are obtained using QE with the optical broadening of 0.1 eV. In order to check the thermodynamic stability of the flat and planar SiC monolayer, ab-initio molecular dynamics (AIMD) calculations are done for an NVT ensemble for 10 ps with a time step of 1.0 fs, using the Nosé-Hoover heat bath approach described by Martyna and Klein [31].

3. Results

In this section, we demonstrate the electronic and optical properties of SiC monolayer for varying planar buckling strength, Δ . The side view of crystal structures of SiC monolayer for different values of Δ is shown in Fig. 1, where the influence of Δ on the atomic positions are clearly seen. The SiC monolayer consists of a combination of carbon atoms known for forming graphene and silicon atoms known to form silicene. It is well known that graphene has a stable planar structure ($\Delta = 0.0$), while the planar buckling of silicene is $\Delta \approx 0.45$ Å [32]. The combination of the C and the Si atoms creates a SiC monolayer with vanishing planar buckling $\Delta = 0.0$. It has been shown that a 2D SiC monolayer has a flat shape with 100% planar structure with inherent dynamic stability [33]. The planar 2D SiC monolayer is thus energetically very stable. Several studies have investigated the stability of a planar SiC monolayer, and all these studies have demonstrated that a 2D SiC is energetically stable and has an inherent dynamic stability [34, 35]. The predicted planarity

property of SiC monolayer is significant in contributing to the development of unprecedented characteristics. In addition, planar buckling plays an important role in controlling the physical properties of SiC monolayer. Understanding the underlying mechanism of the buckling behavior in SiC monolayer is important for the design of siligraphene and its composites. We therefore explore the buckling effects and the mechanisms that modify the SiC monolayer due to the planar buckling [36].

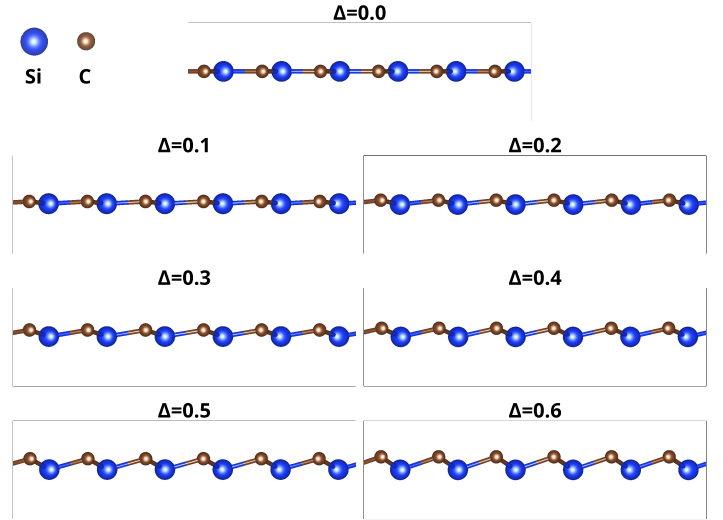


Figure 1: Side view of crystal structures of SiC monolayer for different values of Δ .

3.1. Electronic properties

The 2D SiC monolayers have a graphene-like honeycomb structure consisting of alternating Si and C atoms. Similar to graphene, the C and the Si atoms form sp^2 hybrid orbital to create the SiC nanosheet. The hybridization order is strongly affected by the value of Δ , which causes an orbital redirection and bond reconstruction.

Table 1: Percentage of orbital contribution in bond character and hybridization bond order.

Δ (Å)	s (%)	p (%)	Hybrid
0.0	33.33	66.66	sp^2
0.1	33.10	66.90	$sp^{2.021}$
0.2	32.47	67.53	$sp^{2.079}$
0.3	31.44	68.56	$sp^{2.180}$
0.4	29.97	70.03	$sp^{2.336}$
0.5	28.07	71.93	$sp^{2.562}$
0.6	25.77	74.23	$sp^{2.88}$

In fact, the planar buckling influences the σ and the π bonds of the SiC monolayer leading to enhanced σ - π common bonds. The sp^2 -hybridization is thus changed towards an sp^3 -hybridization for increasing value of Δ as is presented in Tab. 1. For instance, the hybridization becomes $sp^{2.88}$ at $\Delta = 0.6$ Å, and the planar buckling

thus reduces the sp^2 overlapping, and the bond symmetry is broken simultaneously. The maximum allowed value of Δ is 0.6 Å for the SiC monolayer, and the hybridization would become $sp^{>3}$ if the value of the planar buckling were further increased to 0.7 Å, which is an impossible state. The sp^3 bonds instead of the usual sp^2 bonds are also found in SiC nanotube structures [37].

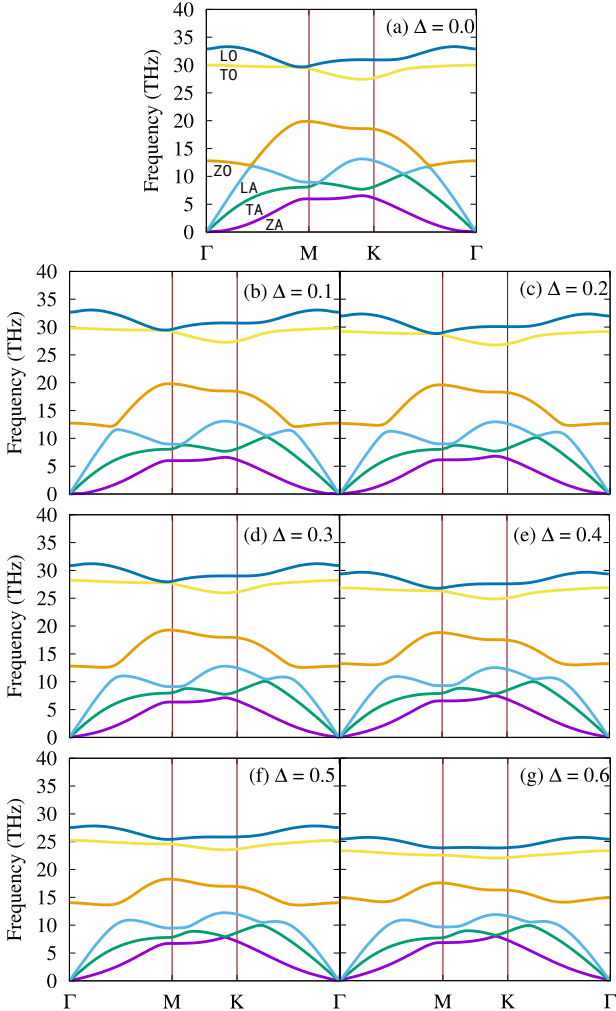


Figure 2: Phonon band structure for different values of $\Delta = 0.0$ (a), 0.1 (b), 0.2 (c), 0.3 (d), 0.4 (e), 0.5 (f), and 0.6 Å (g).

The formation energy, the Si-C bond length, and the band gap are influenced by the planar buckling as is presented in Tab. 2 [38]. The formation energy is the energy required for generating the configuration of a monolayer.

The formation energy of the buckled SiC monolayers is determined relative to a flat layer

$$E_f = E_{\text{Buckling}} - E_{\text{Flat}}, \quad (1)$$

where E_{Buckling} indicates the total energy of a SiC monolayer with planar buckling, and E_{Flat} defines the total energy of the flat SiC monolayer, without buckling. The low formation energy is an indication of the high energetic stability of the SiC monolayer. The lower the formation

energy, the more stable structure is obtained. We can therefore see that the planar SiC monolayer is the most energetically stable structure, and the stability is slightly decreased with increasing Δ .

Table 2: The formation energy (E_f), the bond length of Si-C, and the band gap (E_g) for different values of planar buckling, Δ .

Δ	E_f (eV/atoms)	Si-C (Å)	E_g (eV)
0.0	-	1.781	2.524
0.1	0.111	1.784	2.452
0.2	0.442	1.792	2.260
0.3	0.999	1.806	2.014
0.4	1.781	1.826	1.755
0.5	2.807	1.850	1.514
0.6	4.105	1.880	1.305

The dynamical stability of an SiC monolayer can be tested using the phonon band structure shown in Fig. 2. The phonon band structure along the high symmetry directions is calculated. The phonon band structure of a flat SiC monolayer, $\Delta = 0.0$ (a), has no imaginary frequencies, displaying the dynamical stability of the monolayer. The phonon modes are classified into acoustic and optical modes. The acoustic phonon modes are in-plane longitudinal acoustic (LA), in-plane transverse acoustic (TA), and out-of-plane acoustic (ZA). In the same way, the optical phonon modes are in-plane longitudinal optical (LO), in-plane transverse optical (TO), and out-of-plane optical (ZO) modes. The phonon band structure of the buckled SiC monolayers does not display any imaginary frequencies showing the dynamical stability, even at high values of the planar buckling.

The structure modification caused by the planar buckling changes the Si-C bond length, while the lattice constant is slightly changed (see Tab. 2). The longer bond lengths indicate that the electrons are less tightly bound to the atoms. In this case, less energy is required to remove an electron from an atom leading to a decreased band gap [39]. The longer bond lengths thus correspond to smaller band gaps. We should expect that the SiC monolayer with $\Delta = 0.6$ Å has the smallest band gap among all the considered values of Δ (see Tab. 2).

The band structure of SiC monolayer shown in Fig. 3 confirms the band gap reduction due to the planar buckling. Our results indicate that a flat SiC monolayer, $\Delta = 0.0$, is a direct band gap semiconductor in contrast to the indirect band gap in bulk SiC. The formation of Dirac cones or the direct band gap of a flat SiC monolayer is attributed to the preservation of the π -conjugate orbitals and the hexagonal symmetry. The calculated direct band gap of a flat SiC monolayer is 2.524 eV using GGA-PBE, which is an underestimated value compared to the band gap of 3-4.8 eV computed with the GW quasi-particle correction, GLLB-SC, method and other approximations [40–42]. Increasing the planar buckling the direct band gap is

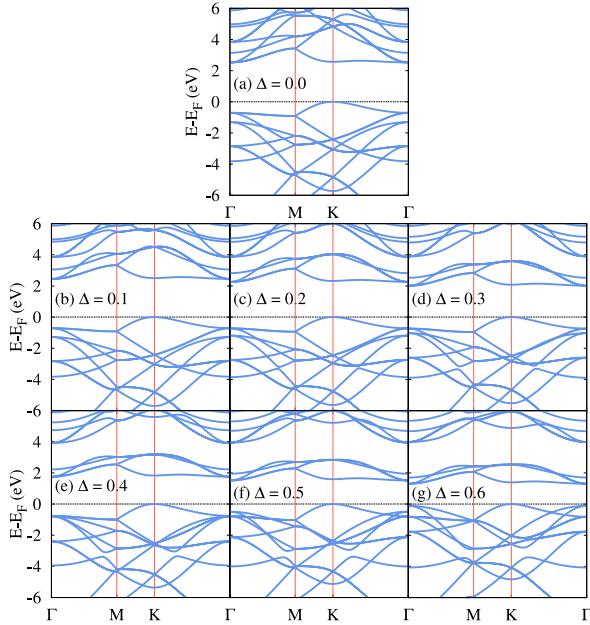


Figure 3: Band structure for optimized SiC monolayers with planer buckling, $\Delta = 0.0$ (a), 0.1 (b), 0.2 (c), 0.3 (d), 0.4 (e), 0.5 (f), and 0.6 Å (g). The energies are with respect to the Fermi level, and the Fermi energy is set to zero.

converted to an indirect band gap with a smaller value especially at $\Delta = 0.6$ Å. The direct-indirect band gap transition can be referred to the destruction of the π -conjugate orbitals and the breaking of the hexagonal symmetry in the presence of planar buckling. The direct-indirect band gap transition phenomena in 2D SiC is also seen in 2D transition metal dichalcogenides (TMDs) [43].

To get insight into the band gap reduction and the band structure modification due to the planar buckling, the partial density of states (PDOS) of a SiC monolayer for different values of Δ is presented in Fig. 4. It is obvious that the density of valence states near the Fermi energy is formed by a hybridization of the p_z -orbitals of Si and C atoms, where the p_z -orbital of the C atoms is dominant for a flat SiC monolayer. In contrast, the density of conduction states near the Fermi energy is generated by a hybridization of the p_z -orbitals of Si and C atoms where the p_z -orbital of the Si atoms is much higher. With increasing Δ , the conduction density of states of the s - and the p -orbital for both the Si and the C atoms moves towards the Fermi energy resulting in a reduction of the semiconducting energy band gap. In addition, the contribution of the s - and $p_{x,y}$ -orbitals of both the Si and the C atoms to the density of states and thus the valence and conduction bands are found with increasing value of Δ . This is an indication that the planar buckling influences the σ and the π bonds of a SiC monolayer leading to enhanced σ - π common bonds in the density of states as well as the band structure.

The electron density distribution describing the valence electron density of a SiC monolayer with different values

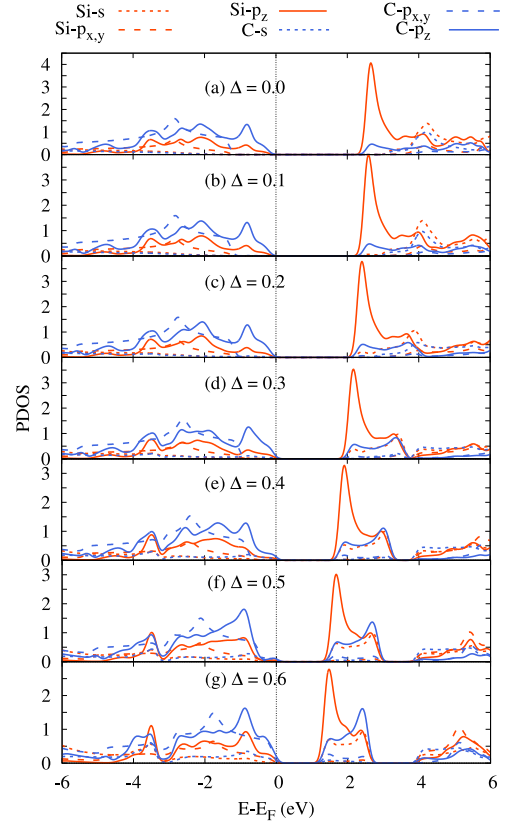


Figure 4: Partial density of states, PDOS of the SiC monolayers with planar buckling, $\Delta = 0.0$ (a), 0.1 (b), 0.2 (c), 0.3 (d), 0.4 (e), 0.5 (f), and 0.6 Å (g). The energies are with respect to the Fermi level, and the Fermi energy is set to zero.

of Δ is presented in Fig. 5 [44]. The Si and the C atoms have $3s^23p^2$ and $2s^22p^2$ valence electrons, respectively. Although the Si and the C atoms have the same number of valence electrons, the distribution of the valence electrons around the Si and the C atoms in a flat SiC monolayer are quite different from each other. The electron density around Si is localized on the atom, whereas that around C is spatially spread. It corresponds to the difference in electronegativities between the C and the Si atoms, where the C atoms are more electronegative than the Si atoms. When the planar buckling increased, the planes of the Si and the C atoms are slightly separated leading to almost the same electron distribution around the Si and the C atoms, but the distribution of the electrons localized around the atoms slightly change their shape (see Fig. 5g). The contributions to the density of states were also modified as a result of the buckling effects. In a flat SiC monolayer, the C atoms used to have a larger charge density than the Si atoms due to their higher electronegativity, while this contribution is altered due to the planar buckling caused by the differences in the bond lengths, which are elongated with Δ . (see Fig. 5g).

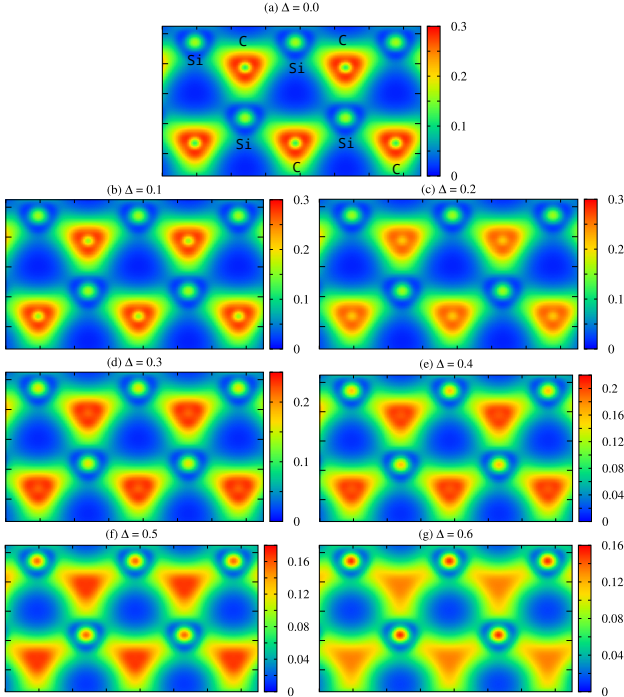


Figure 5: Electron density of SiC monolayers with planar buckling, $\Delta = 0.0$ (a), 0.1 (b), 0.2 (c), 0.3 (d), 0.4 (e), 0.5 (f), and 0.6 Å (g).

3.2. Mechanical responses

Based on the investigation of stable structures, the mechanical response under uniaxial strain along either the armchair or zigzag direction can be calculated. The buckling parameter influences the Si-C bond length, and the modifications of bond lengths affect the mechanical properties of the SiC monolayer. The stress-strain curves of the flat and buckled SiC monolayers are displayed in Fig. 6 for the Zigzag direction of the structure. The mechanical response along the armchair direction is very similar to the one in the zigzag direction due to the symmetric properties of the SiC monolayer in both the x - and the y -direction, we thus provide only the stress-strain curve along the zigzag direction.

Our stress-strain curve for flat SiC monolayer is consistent with those existing in the literature, indicating the reliability of the present computational scheme [45]. Similar to previous DFT studies on 2D materials [46], all monolayer structures with different stoichiometry also obey linear relationships with strain within a small strain range, and deviate from the linear elasticity under large deformation. The ultimate tensile strength for a flat SiC is found to be 20.38 N/m, and the fracture point is 15.8%. The fracture point can be defined as the point of strain where the monolayer separates. At the fracture point, the strain approaches its maximum value, and the monolayer fractures, even though the corresponding stress may be less than the ultimate strength at this point.

In the presence of planar buckling, both the ultimate tensile strength and the values for the fracture point are extremely decreased (inset) in such away that the ulti-

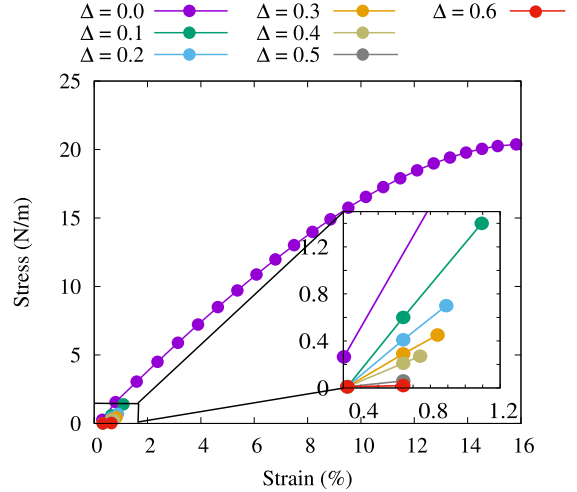


Figure 6: Stress strain curve of the SiC monolayer with buckling parameter, $\Delta = 0.0$ (purple), 0.1 (green), 0.2 (light blue), 0.3 (orange), 0.4 (olive), 0.4 (light brown), 0.5 (gray), and 0.6 Å (red) in the case of E_{\parallel} (a), and E_{\perp} (b). The vertical black and red lines show different regions of the electromagnetic spectrum.

mate tensile strength and the fracture point are inversely proportional to the planar buckling. This is caused by the fact that the planar buckling increases the Si-C bond length, and longer bond length will break easier. Consequently, the buckled SiC monolayer has a lower mechanical response under a uniaxial strain.

3.3. Thermal properties

In this section, thermal properties such as the heat capacity are presented in addition to the temperature-time curve for the flat and planar SiC monolayers. The thermal stability is calculated up to 10 ps with a time step of 1.0 fs as is demonstrated in Fig. 7. The temperature curve of the pure and the buckled SiC monolayers neither displays large fluctuations in the temperature nor serious structure disruptions or bond breaking at 300 K. This indicates that the pure and the buckled SiC monolayers are thermodynamically stable nanosheets.

The heat capacity defines the ratio of the heat absorbed by a material to the temperature change. The heat capacity of a flat and a buckled SiC are shown in Fig. 8. The heat capacity increases with temperature, but becomes almost constant at high values of temperature, $T > 700$ K. It is expected to have higher heat capacity for the systems with stronger bonds, which is a predicted trend for the heat capacity consistent with the classical theory [47]. This means that a higher heat capacity can be obtained from a stronger bond structure. In fact, a bond becomes stronger if the electronegativity difference across the bond increases. In our buckled monolayers, the buckling does not much affect the electronegativity difference across a bond, and the strength of the bonds is thus almost unchanged with increasing buckling parameter. Consequently, the heat capacity is slightly changed with the buckling parameter as

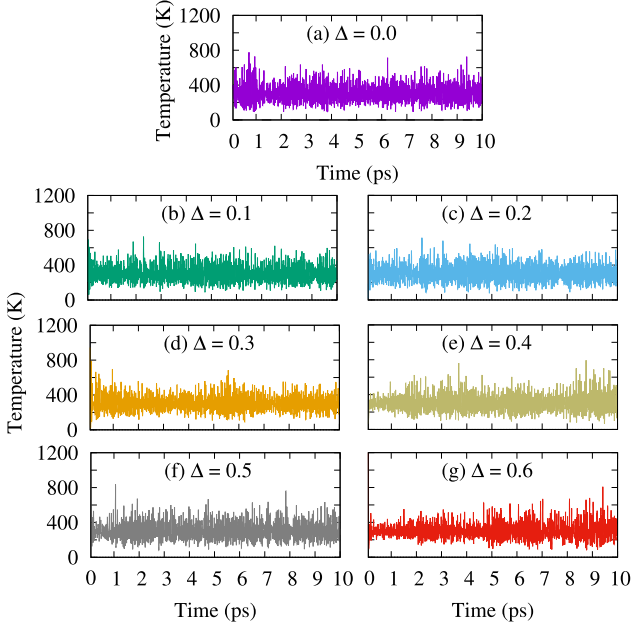


Figure 7: Temperature versus the AIMD simulation time steps at 300 K for optimized SiC monolayers with planar buckling, $\Delta = 0.0$ (a), 0.1 (b), 0.2 (c), 0.3 (d), 0.4 (e), 0.5 (f), and 0.6 Å (g).

shown in Fig. 8. This indicates that the thermal properties such as heat capacity are not sensitive to the buckling parameter.

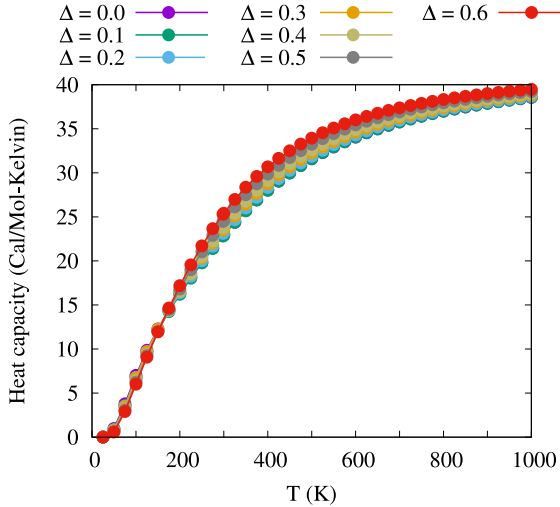


Figure 8: Heat capacity of the SiC monolayer with buckling parameter, $\Delta = 0.0$ (purple), 0.1 (green), 0.2 (light blue), 0.3 (orange), 0.4 (olive), 0.4 (light brown), 0.5 (gray), and 0.6 Å (red).

3.4. Optical properties

Next, the optical properties of a SiC monolayer in relation to the planar buckling are investigated. The dielectric function, the absorption coefficient, and the optical conductivity are all calculated using the random phase approximation (RPA) [48]. In order to achieve great accuracy, the RPA in the QE package employs a dense

$100 \times 100 \times 1$ mesh grid in the Brillouin zone [49]. For parallel (E_{\parallel}) and perpendicular (E_{\perp}) polarization of the incoming electric field, the imaginary, $\text{Im}(\varepsilon)$, and the real, $\text{Re}(\varepsilon)$, components of the dielectric function are shown in the Fig. 9.

In the case of E_{\parallel} , a significant peak in $\text{Im}(\varepsilon)$ for flat SiC monolayer starts to be produced at 2.5 eV and it reaches maximum value at 3.2 eV in the visible close to the near-UV spectrum as is presented in Fig. 9a (purple line). This is in accordance with previous findings [50] for a stable planar structure. The result indicated that this value is associated with the SiC's electronic band gap, confirming that SiC is a semiconductor.

As Δ is increased, the peak moves to lower energy, when the incoming electric field is polarized in parallel (E_{\parallel}). The major peak, which corresponds to the optical band gap, has been shifted down to the deep visible and the near-IR areas. The shift of the peak implies the appearance of additional states close to the Fermi energy. This finding is advantageous for optoelectronic devices that work with visible light. On the other hand, as a result of the change in the band structure, as well as the emergence of a shift in the band gap's direction, the peak's intensity is increased. The illustrated electromagnetic spectrum regimes for $\text{Im}(\varepsilon)$ show a considerable tuning to lower energy with increasing Δ for the case of (E_{\perp}).

The real component of the dielectric function is associated to a variety of fascinating physical phenomena, such as the static dielectric constant and the plasmon energy of the SiC monolayer. The real component of the dielectric function at zero energy, also known as the static dielectric constant $\text{Re}(\varepsilon(0))$, is another significant quantity to consider. Because the value of $\text{Re}(\varepsilon(\omega))$ is inversely related to the band gap, $\text{Re}(\varepsilon(\omega)) \approx 1/E_g$, the value of $\text{Re}(\varepsilon(0))$ increases with Δ [51]. With increasing Δ , the band gap is narrowed, and the value of $\text{Re}(\varepsilon(0))$ rises. $\text{Re}(\varepsilon)$ increases faster for E_{\parallel} than for E_{\perp} , showing that $\text{Re}(\varepsilon)$ exhibits an anisotropy regarding the polarization of the incoming field.

Another interesting phenomena are the plasmons which are connected to both the imaginary and the real components of the dielectric function. The plasmons are a group of valence or conduction electrons in a material participating in collective oscillations. The real component of a material's complex dielectric function depicts the electromagnetic wave transmission across the medium, whereas the imaginary component describes single particle excitations, which are characterized by interband transitions [52, 53]. At a plasmon energy, the real part of dielectric function is zero, while the imaginary part has a maximum value. So, the real component of the dielectric function changes its sign from positive to negative at the plasmon frequency, as well as at the plasmon energy. In the case of E_{\parallel} , the plasmon energy of a flat SiC monolayer stays unchanged and does not pass the negative sign. It indicates that the flat SiC monolayer does not support plasmonic oscillations in the selected energy range of the applied electromagnetic wave. When Δ grows, the plasmon energy appears

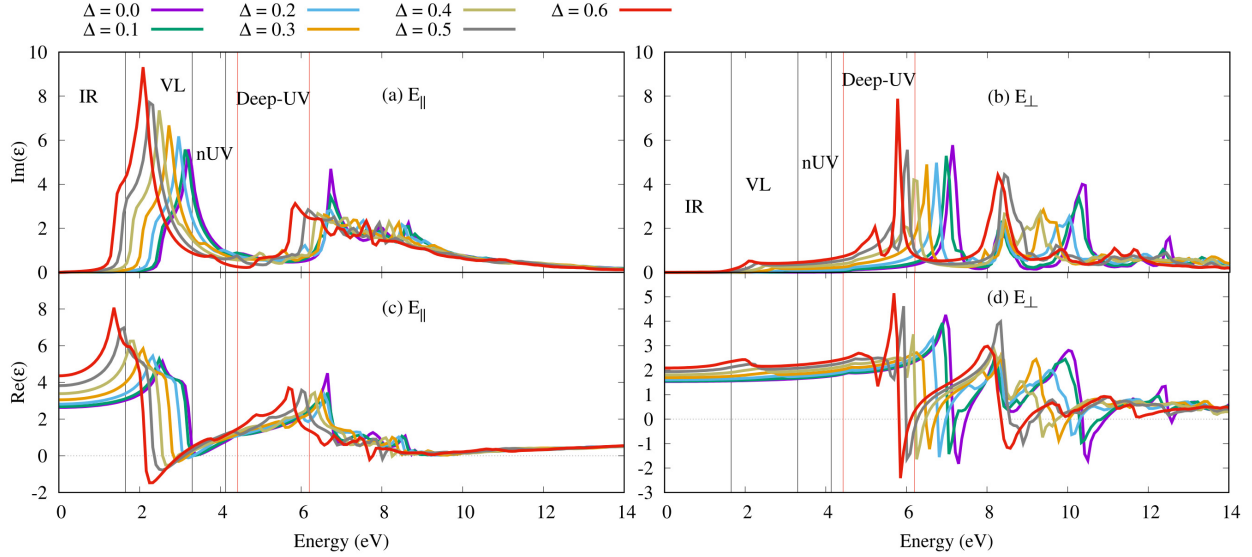


Figure 9: Imaginary, $\text{Im}(\epsilon)$, (a,b) and real, $\text{Re}(\epsilon)$, (c,d) parts of dielectric function for the SiC monolayer with buckling parameter, $\Delta = 0.0$ (purple), 0.1 (green), 0.2 (light blue), 0.3 (orange), 0.4 (olive), 0.5 (gray), and 0.6 Å (red) in the case of E_{\parallel} (left panel), and E_{\perp} (right panel). The vertical black and red lines show different regions of electromagnetic wave.

at $\Delta = 0.2$ Å and the plasmon energy shifts to a lower energy scale, indicated by the real part of the dielectric function crossing the zero point assuming negative values, indicating that the electrons in a SiC monolayer exhibit plasmonic behavior with increasing Δ , as is shown in Fig. 9. The same mechanism can be applied to the plasmonic behavior when E_{\perp} is considered.

Next, the information on the electronic band structures in combination with the incoming field E_{\parallel} (a) and E_{\perp} (b) are used to determine the actual components of the optical conductivity spectra for buckled and planar SiC monolayers. For SiC monolayers with planar structures below 2.5 eV (E_{\parallel}) and 4.2 eV (E_{\perp}), σ_{optical} is 0 as is shown in Fig. 10, and the change follows the same pattern as the change in the dielectric function. The first intense peak of flat SiC monolayer in σ_{optical} for E_{\parallel} and E_{\perp} is found at 3.2 ($\sigma_{\text{optical}} = 1.42$) and 7.13 eV ($\sigma_{\text{optical}} = 3.3$), respectively, which is in a good agreement with previous studies of flat SiC monolayer [54], when noticing that the value of the optical conductivity of our SiC monolayer is smaller due to different size of our supercell.

The visible region of E_{\parallel} exhibits a strong peak, and the intensity of the maximum is slightly increased as Δ increases, but its position is dislocated to lower energy, revealing the optical band gap. In addition, there is a significant peak in the UV region at high photon energy 6-8 eV, which corresponds to the transitions of to higher energy levels. The peak's intensity is quite high for flat SiC monolayers in this area, but it is decreased by Δ and moves to the deep visible region, a new conduction mechanism arises. Moreover, when planar buckling is intensified, the polarization direction of the incoming light has a major impact on the optical conductivity, in the case of E_{\perp} . Increased planar buckling alters the structure of

the spectra, allowing direct transitions, while maintaining the crystal momentum direct without a significant change in the wave vector.

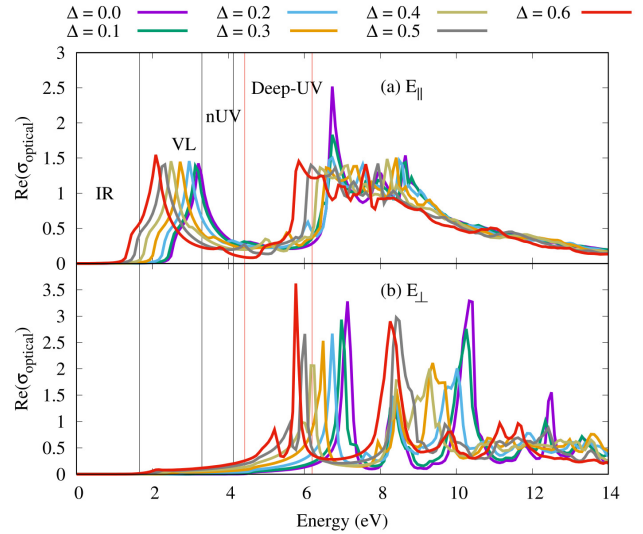


Figure 10: Optical conductivity (real part) of the SiC monolayer with buckling parameter, $\Delta = 0.0$ (purple), 0.1 (green), 0.2 (light blue), 0.3 (orange), 0.4 (olive), 0.4 (light brown), 0.5 (gray), and 0.6 Å (red) in the case of E_{\parallel} (a), and E_{\perp} (b). The vertical black and red lines show different regions of the electromagnetic spectrum.

Our final goal is the absorption spectra presented in Fig. 11, which displays the absorption coefficient of a SiC monolayer versus energy for both polarizations in a flat structure and layers with different levels of planar buckling. In contrast to the optical conductivity, intensity of the main peak in the absorption spectra located around 2.0-4.0 eV for E_{\parallel} is slightly decreased with Δ .

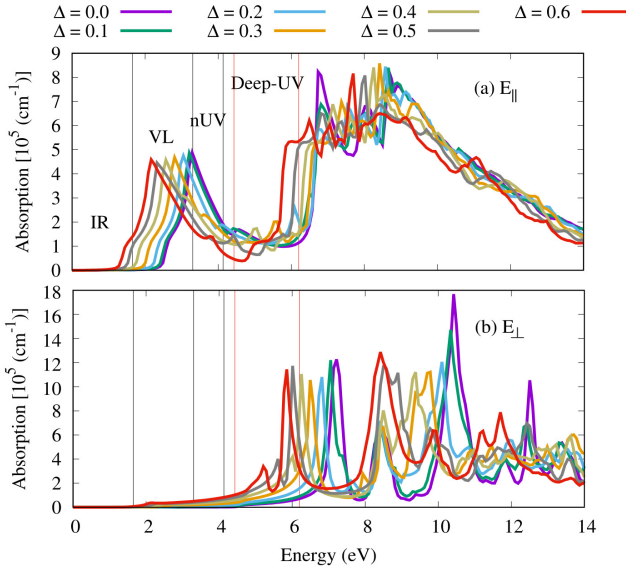


Figure 11: Absorption coefficient of the SiC monolayer with buckling parameter, $\Delta = 0.0$ (purple), 0.1 (green), 0.2 (light blue), 0.3 (orange), 0.4 (olive), 0.5 (gray) and 0.6 Å (red) in the case of $E_{||}$ (a), and E_{\perp} (b). The vertical black and red lines show different regions of the electromagnetic spectrum.

4. Conclusions

The electronic structure and optical properties of a SiC monolayer are studied using density functional theory calculation for a varying degree of the planar buckling. With an increase in Δ , the band structure changes and the band gap is narrowed. The contributions to the density of states are modified as a result of the buckling effects. In a flat SiC monolayer, the C atoms have a larger charge density than the Si atoms due to their higher electronegativity, however this contribution varies due to planar buckling causing changes in the bond lengths. Parallel and perpendicular polarization of incoming electric fields with respect to the plane of the SiC monolayer are employed to explore the optical characteristics of the SiC monolayer. With increasing buckling strength, the optical spectra are enhanced for both polarizations. There are shifts for the two main peaks of the real and the imaginary parts of the dielectric function changing from the Deep-UV to the near visible area owing to the appearance of σ - π bonds in the sp^3 hybridization. Small peaks are related to the electronic band gap and the system remains a semiconductor as the band gap narrows, but strong peaks are associated with interband transitions owing to the frequency dependence of the real component of conductivity. As a result, the optical characteristics can be tuned by changing the planar buckling in the visible region. A flat SiC monolayer exhibits good optical properties in the near visible area, whereas the absorption region is changed by increasing planar buckling from the near to the far visible region, resulting in a stronger σ - π bond. The SiC siligraphene is a flexible material that can be used in the applications of smart nanomaterial in which the findings are remarkable.

5. Acknowledgment

The University of Sulaimani and the Research Center of Komar University of Science and Technology provided financial assistance for this project. The calculations were carried out using resources given by the University of Sulaimani's Division of Computational Nanoscience.

References

- [1] A. Gupta, T. Sakhivel, S. Seal, Recent development in 2D materials beyond graphene, *Progress in Materials Science* 73 (2015) 44–126.
- [2] B. Peng, P. K. Ang, K. P. Loh, Two-dimensional dichalcogenides for light-harvesting applications, *Nano Today* 10 (2) (2015) 128–137.
- [3] N. R. Abdullah, B. J. Abdullah, C.-S. Tang, V. Gudmundsson, Properties of BC_6N monolayer derived by first-principle computation: Influences of interactions between dopant atoms on thermoelectric and optical properties, *Materials Science in Semiconductor Processing* 135 (2021) 106073.
- [4] K. S. Novoselov, A. K. Geim, S. V. Morozov, D.-e. Jiang, Y. Zhang, S. V. Dubonos, I. V. Grigorieva, A. A. Firsov, Electric field effect in atomically thin carbon films, *Science* 306 (5696) (2004) 666–669.
- [5] K. F. Mak, J. Shan, Photonics and optoelectronics of 2D semiconductor transition metal dichalcogenides, *Nature Photonics* 10 (4) (2016) 216–226.
- [6] P. Vogt, P. De Padova, C. Quaresima, J. Avila, E. Frantzeskakis, M. C. Asensio, A. Resta, B. Ealet, G. Le Lay, Silicene: Compelling experimental evidence for graphenelike two-dimensional silicon, *Physical review letters* 108 (15) (2012) 155501.
- [7] A. J. Mannix, Z. Zhang, N. P. Guisinger, B. I. Yakobson, M. C. Hersam, Borophene as a prototype for synthetic 2D materials development, *Nature nanotechnology* 13 (6) (2018) 444–450.
- [8] F.-f. Zhu, W.-j. Chen, Y. Xu, C.-l. Gao, D.-d. Guan, C.-h. Liu, D. Qian, S.-C. Zhang, J.-f. Jia, Epitaxial growth of two-dimensional stanene, *Nature materials* 14 (10) (2015) 1020–1025.
- [9] F. Zheng, H. Dong, Y. Ji, Y. Li, Adsorption of hydrazine on XC_3 ($X = B, Al, N, Si, \text{ and } Ge$) nanosheets: A computational study, *International Journal of Hydrogen Energy* 44 (12) (2019) 6055–6064.
- [10] E. Anikina, T. Hussain, V. Beskachko, R. Ahuja, Elucidating hydrogen storage properties of two-dimensional siligraphene (SiC_8) monolayers upon selected metal decoration, *Sustainable Energy & Fuels* 4 (11) (2020) 5578–5587.
- [11] M. Houmad, A. El Kenz, A. Benyoussef, Thermal and electrical properties of siligraphene and its derivatives, *Optik* 157 (2018) 936–943.
- [12] J. Guan, L. Zhang, K. Deng, Y. Du, E. Kan, Computational dissection of 2D SiC_7 monolayer: a direct band gap semiconductor and high power conversion efficiency, *Advanced Theory and Simulations* 2 (8) (2019) 1900058.
- [13] M. Houmad, H. Zaari, A. Benyoussef, A. El Kenz, Optical properties of titanium and iron doped 3C-SiC behaviors Tb-Mbj, *Chinese journal of physics* 54 (6) (2016) 960–967.
- [14] N. R. Abdullah, G. A. Mohammed, H. O. Rashid, V. Gudmundsson, Electronic, thermal, and optical properties of graphene like six structures: Significant effects of Si atom configurations, *Physics Letters A* 384 (24) (2020) 126578.
- [15] S. Lin, Light-emitting two-dimensional ultrathin silicon carbide, *The Journal of Physical Chemistry C* 116 (6) (2012) 3951–3955.
- [16] S. Chabi, H. Chang, Y. Xia, Y. Zhu, From graphene to silicon carbide: ultrathin silicon carbide flakes, *Nanotechnology* 27 (7) (2016) 075602.
- [17] J. Chen, N. Li, Y. Wei, B. Han, Y. Zhang, A low-cost approach to fabricate SiC nanosheets by reactive sintering from Si powders and graphite, *Journal of Alloys and Compounds* 788 (2019) 345–351.

- [18] S. Chabi, Z. Guler, A. J. Brearley, A. D. Benavidez, T. S. Luk, The creation of true two-dimensional silicon carbide, *Nanomaterials* 11 (7) (2021) 1799.
- [19] A. Majid, N. Rani, S. U.-D. Khan, Z. A. Almutairi, First principles study of structural, electronic and magnetic properties of transition metals doped SiC monolayers for applications in spintronics, *Journal of Magnetism and Magnetic Materials* 503 (2020) 166648.
- [20] Y. Wan-Jun, Q. Xin-Mao, Z. Chun-Hong, Z. Zhong-Zheng, Z. Shi-Yun, Photoelectric properties of La, Ce, Th doped 2D SiC: A first principle study, *J. Nanomater. Mol. Nanotechnol* 2018 (2019) 10.
- [21] Z. Xu, Y. Li, Z. Liu, Controlling electronic and optical properties of layered SiC and GeC sheets by strain engineering, *Materials & Design* 108 (2016) 333–342.
- [22] N. R. Abdullah, H. O. Rashid, C.-S. Tang, A. Manolescu, V. Gudmundsson, Controlling physical properties of bilayer graphene by stacking orientation caused by interaction between B and N dopant atoms, *Materials Science and Engineering: B* 276 (2022) 115554. doi:<https://doi.org/10.1016/j.mseb.2021.115554>. URL <https://www.sciencedirect.com/science/article/pii/S0921510721005080>
- [23] S. Belarouci, T. Ouahrani, N. Benabdallah, A. Morales-Garcia, I. Belabbas, Two-dimensional silicon carbide structure under uniaxial strains, electronic and bonding analysis, *Computational Materials Science* 151 (2018) 288–295.
- [24] Z. Zhao, Y. Yong, R. Gao, S. Hu, Q. Zhou, Y. Kuang, Enhancement of Nitride-GaS sensing performance of sic7 monolayer induced by external electric field, *Vacuum* 191 (2021) 110393.
- [25] N. Delavari, M. Jafari, Electronic and optical properties of hydrogenated silicon carbide nanosheets: A DFT study, *Solid State Communications* 275 (2018) 1–7.
- [26] J. Jalilian, M. Safari, S. Naderizadeh, Buckling effects on electronic and optical properties of BeO monolayer: First principles study, *Computational Materials Science* 117 (2016) 120–126.
- [27] N. R. Abdullah, B. J. Abdullah, C.-S. Tang, V. Gudmundsson, Enhanced ultraviolet absorption in BN monolayers caused by tunable buckling, arXiv preprint [arXiv:2201.00116](https://arxiv.org/abs/2201.00116) (2022).
- [28] G. Kresse, J. Furthmüller, Efficient iterative schemes for ab initio total-energy calculations using a plane-wave basis set, *Phys. Rev. B* 54 (1996) 11169–11186. doi:[10.1103/PhysRevB.54.11169](https://doi.org/10.1103/PhysRevB.54.11169). URL <https://link.aps.org/doi/10.1103/PhysRevB.54.11169>
- [29] P. Giannozzi, S. Baroni, N. Bonini, M. Calandra, R. Car, C. Cavazzoni, D. Ceresoli, G. L. Chiarotti, M. Cococcioni, I. Dabo, A. D. Corso, S. de Gironcoli, S. Fabris, G. Fratesi, R. Gebauer, U. Gerstmann, C. Gougoussis, A. Kokalj, M. Lazzeri, L. Martin-Samos, N. Marzari, F. Mauri, R. Mazzarello, S. Paolini, A. Pasquarello, L. Paulatto, C. Sbraccia, S. Scandolo, G. Sclauzero, A. P. Seitsonen, A. Smogunov, P. Umari, R. M. Wentzcovitch, QUANTUM ESPRESSO: a modular and open-source software project for quantum simulations of materials, *Journal of Physics: Condensed Matter* 21 (39) (2009) 395502. doi:[10.1088/0953-8984/21/39/395502](https://doi.org/10.1088/0953-8984/21/39/395502). URL <https://doi.org/10.1088/0953-8984/21/39/395502>
- [30] P. Giannozzi, O. Andreussi, T. Brumme, O. Bunau, M. B. Nardelli, M. Calandra, R. Car, C. Cavazzoni, D. Ceresoli, M. Cococcioni, et al., Advanced capabilities for materials modelling with quantum espresso, *Journal of Physics: Condensed Matter* 29 (46) (2017) 465901.
- [31] G. J. Martyna, M. L. Klein, M. Tuckerman, Nosé–hoover chains: The Journal of Chemical Physics 97 (4) (1992) 2635–2643. arXiv:[https://doi.org/10.1063/1.463940](https://arxiv.org/abs/https://doi.org/10.1063/1.463940), doi:[10.1063/1.463940](https://doi.org/10.1063/1.463940). URL <https://doi.org/10.1063/1.463940>
- [32] N. R. Abdullah, M. T. Kareem, H. O. Rashid, A. Manolescu, V. Gudmundsson, Spin-polarised DFT modeling of electronic, magnetic, thermal and optical properties of silicene doped with transition metals, *Physica E: Low-dimensional Systems and Nanostructures* 129 (2021) 114644. doi:<https://doi.org/10.1016/j.physe.2021.114644>. URL <https://www.sciencedirect.com/science/article/pii/S1386947721000266>
- [33] S. Chabi, H. Chang, Y. Xia, Y. Zhu, From graphene to silicon carbide: ultrathin silicon carbide flakes, *Nanotechnology* 27 (7) (2016) 075602. doi:[10.1088/0957-4484/27/7/075602](https://doi.org/10.1088/0957-4484/27/7/075602). URL <https://doi.org/10.1088/0957-4484/27/7/075602>
- [34] S. Chabi, K. Kadel, Two-dimensional silicon carbide: Emerging direct band gap semiconductor, *Nanomaterials* 10 (11) (2020). doi:[10.3390/nano10112226](https://doi.org/10.3390/nano10112226). URL <https://www.mdpi.com/2079-4991/10/11/2226>
- [35] S. S. Lin, Light-emitting two-dimensional ultrathin silicon carbide, *The Journal of Physical Chemistry C* 116 (6) (2012) 3951–3955. arXiv:<https://doi.org/10.1021/jp210536m>, doi:[10.1021/jp210536m](https://doi.org/10.1021/jp210536m). URL <https://doi.org/10.1021/jp210536m>
- [36] N. R. Abdullah, B. J. Abdullah, H. O. Rashid, C.-S. Tang, V. Gudmundsson, Study of the buckling effects on the electrical and optical properties of the group III-Nitride monolayers, *Materials Science in Semiconductor Processing* 150 (2022) 106943. doi:<https://doi.org/10.1016/j.mssp.2022.106943>. URL <https://www.sciencedirect.com/science/article/pii/S1369800122004772>
- [37] Y.-L. Shi, J.-M. Zhang, K.-W. Xu, Structural and electronic properties of SiC nanotubes filled with Cu nanowires: A first-principles study, *Physica E: Low-dimensional Systems and Nanostructures* 54 (2013) 319–325. doi:<https://doi.org/10.1016/j.physe.2013.07.021>. URL <https://www.sciencedirect.com/science/article/pii/S1386947713002622>
- [38] N. R. Abdullah, B. J. Abdullah, V. Gudmundsson, DFT study of tunable electronic, magnetic, thermal, and optical properties of a Ga_2Si_6 monolayer, *Solid State Sciences* 125 (2022) 106835. doi:<https://doi.org/10.1016/j.solidstatesciences.2022.106835>. URL <https://www.sciencedirect.com/science/article/pii/S1293255822000309>
- [39] Z. Gacevic, P. Lefebvre, F. Bertram, G. Schmidt, P. Veit, J. Christen, E. Calleja, Growth and Characterization of In-GaN/GaN Quantum Dots for violet-blue Applications, 9th International Conference on Nitride Semiconductors - ICNS9., poster (Jul 2011). URL <https://hal.archives-ouvertes.fr/hal-00632224>
- [40] N. Alaal, V. Loganathan, N. Medhekar, A. Shukla, First principles many-body calculations of electronic structure and optical properties of SiC nanoribbons, *Journal of Physics D: Applied Physics* 49 (10) (2016) 105306. doi:[10.1088/0022-3727/49/10/105306](https://doi.org/10.1088/0022-3727/49/10/105306). URL <https://doi.org/10.1088/0022-3727/49/10/105306>
- [41] H. C. Hsueh, G. Y. Guo, S. G. Louie, Excitonic effects in the optical properties of a sic sheet and nanotubes, *Phys. Rev. B* 84 (2011) 085404. doi:[10.1103/PhysRevB.84.085404](https://doi.org/10.1103/PhysRevB.84.085404). URL <https://link.aps.org/doi/10.1103/PhysRevB.84.085404>
- [42] E. Bekaroglu, M. Topsakal, S. Cahangirov, S. Ciraci, First-principles study of defects and adatoms in silicon carbide honeycomb structures, *Phys. Rev. B* 81 (2010) 075433. doi:[10.1103/PhysRevB.81.075433](https://doi.org/10.1103/PhysRevB.81.075433). URL <https://link.aps.org/doi/10.1103/PhysRevB.81.075433>
- [43] H. Şahin, S. Cahangirov, M. Topsakal, E. Bekaroglu, E. Akturk, R. T. Senger, S. Ciraci, Monolayer honeycomb structures of group-IV elements and III-V binary compounds: First-principles calculations, *Phys. Rev. B* 80 (2009) 155453. doi:[10.1103/PhysRevB.80.155453](https://doi.org/10.1103/PhysRevB.80.155453). URL <https://link.aps.org/doi/10.1103/PhysRevB.80.155453>
- [44] N. R. Abdullah, B. J. Abdullah, V. Gudmundsson, High thermoelectric and optical conductivity driven by the interaction of boron and nitrogen dopant atoms with a 2D monolayer beryl-

- lium oxide, *Materials Science in Semiconductor Processing* 141 (2022) 106409. doi:<https://doi.org/10.1016/j.mssp.2021.106409>.
URL <https://www.sciencedirect.com/science/article/pii/S136980012100740X>
- [45] X. K. Lu, T. Y. Xin, Q. Zhang, Q. Xu, T. H. Wei, Y. X. Wang, Versatile mechanical properties of novel g- SiC_x monolayers from graphene to silicene: a first-principles study, *Nanotechnology* 29 (31) (2018) 315701. doi:[10.1088/1361-6528/aac337](https://doi.org/10.1088/1361-6528/aac337).
URL <https://doi.org/10.1088/1361-6528/aac337>
- [46] Z. G. Fthenakis, N. N. Lathiotakis, Graphene allotropes under extreme uniaxial strain: an ab initio theoretical study, *Phys. Chem. Chem. Phys.* 17 (2015) 16418–16427. doi:[10.1039/C5CP02412A](https://doi.org/10.1039/C5CP02412A).
URL <http://dx.doi.org/10.1039/C5CP02412A>
- [47] B. Mortazavi, F. Shojaei, T. Rabczuk, X. Zhuang, High tensile strength and thermal conductivity in BeO monolayer: A first-principles study, *FlatChem* 28 (2021) 100257. doi:<https://doi.org/10.1016/j.flatc.2021.100257>.
URL <https://www.sciencedirect.com/science/article/pii/S2452262721000362>
- [48] X. Ren, P. Rinke, C. Joas, M. Scheffler, Random-phase approximation and its applications in computational chemistry and materials science, *Journal of Materials Science* 47 (21) (2012) 7447–7471.
- [49] H. Ehrenreich, M. H. Cohen, Self-consistent field approach to the many-electron problem, *Phys. Rev.* 115 (1959) 786–790. doi:[10.1103/PhysRev.115.786](https://doi.org/10.1103/PhysRev.115.786).
URL <https://link.aps.org/doi/10.1103/PhysRev.115.786>
- [50] S. Majidi, N. B. Nezafat, D. Rai, A. Achour, H. Ghaziasadi, A. Sheykhan, S. Solaymani, Optical and electronic properties of pure and fully hydrogenated SiC and GeC nanosheets: first-principles study, *Optical and Quantum Electronics* 50 (7) (2018) 1–13.
- [51] D. R. Penn, Wave-number-dependent dielectric function of semiconductors, *Phys. Rev.* 128 (1962) 2093–2097. doi:[10.1103/PhysRev.128.2093](https://doi.org/10.1103/PhysRev.128.2093).
URL <https://link.aps.org/doi/10.1103/PhysRev.128.2093>
- [52] H. Raether, Excitation of plasmons and interband transitions by electrons, Vol. 88, Springer, 2006.
- [53] R. Egerton, An introduction to eels, in: *Electron Energy-Loss Spectroscopy in the Electron Microscope*, Springer, 2011, pp. 1–28.
- [54] M. Houmad, O. Dakir, A. Abbassi, A. Benyoussef, A. El Kenz, H. Ez-Zahraouy, Optical properties of sic nanosheet, *Optik* 127 (4) (2016) 1867–1870. doi:<https://doi.org/10.1016/j.ijleo.2015.11.017>.
URL <https://www.sciencedirect.com/science/article/pii/S0030402615016253>